NASA TECHNICAL NOTE

NASA TN D-8289

NASA TN D-8289

BORON-EPOXY-REINFORCED TITANIUM AIRCRAFT LANDING-GEAR DRAG STRUT

William E. Howell

Langley Research Center
Hampton, Va. 23665

NATIONAL AERONAUTICS AND SPACE ADMINISTRATION · WASHINGTON, D. C. · NOVEMBER 1976

1. Report No.	2. Government Accession No.	3. Recipient's Catalog No.
NASA TN D-8289		

4. Title and Subtitle	5. Report Date
BORON-EPOXY-REINFORCED TITANIUM AIRCRAFT LANDING-GEAR DRAG STRUT	November 1976
	6. Performing Organization Code

7. Author(s)	8. Performing Organization Report No.
William E. Howell	L-10527
	10. Work Unit No.
	505-02-41-01

9. Performing Organization Name and Address	11. Contract or Grant No.
NASA Langley Research Center Hampton, VA 23665	
	13. Type of Report and Period Covered
	Technical Note

12. Sponsoring Agency Name and Address	14. Sponsoring Agency Code
National Aeronautics and Space Administration Washington, DC 20546	

15. Supplementary Notes

16. Abstract

The structural performance of a boron-epoxy-reinforced titanium drag strut, containing a bonded scarf joint and designed to the criteria of a large commercial transport, has been evaluated experimentally and analytically. The strut was exposed to two lifetimes of fatigue loading and was statically loaded to the tensile and compressive design ultimate loads. Throughout the test program no evidence of any damage in the drag strut was detected by strain-gage measurements, ultrasonic inspection, or visual observation. The bonded joint was analyzed using the NASTRAN® (NASA Structural Analysis) computer program. A comparison of the strains predicted by the NASTRAN computer program with the experimentally determined values shows excellent agreement. An analytical study indicated that the nonlinear behavior of a structural spacer at each end of the strut could be explained by the inelastic behavior and possible creep of the adhesive.

17. Key Words (Suggested by Author(s))	18. Distribution Statement
Boron-epoxy Bonded joints Composites Landing-gear components	Unclassified - Unlimited Subject Category 27

19. Security Classif. (of this report)	20. Security Classif. (of this page)	21. No. of Pages	22. Price*
Unclassified	Unclassified	31	$3.75

* For sale by the National Technical Information Service, Springfield, Virginia 22161

BORON-EPOXY-REINFORCED TITANIUM AIRCRAFT LANDING-GEAR DRAG STRUT

William E. Howell
Langley Research Center

SUMMARY

The structural performance of a boron-epoxy-reinforced titanium drag strut, containing a bonded scarf joint and designed to the criteria of a large commercial transport, has been evaluated experimentally and analytically. The strut was exposed to two lifetimes of fatigue loading and was statically loaded to the tensile and compressive design ultimate loads. Throughout the test program no evidence of any damage in the drag strut was detected by strain-gage measurements, ultrasonic inspection, or visual observation. The bonded joint was analyzed using the NASTRAN® (NASA Structural Analysis) computer program. A comparison of the strains predicted by the NASTRAN computer program with the experimentally determined values shows excellent agreement. An analytical study indicated that the nonlinear behavior of a structural spacer at each end of the strut could be explained by the inelastic behavior and possible creep of the adhesive.

INTRODUCTION

Aircraft designers are continually endeavoring to develop more efficient structures. The use of high modulus fibers, such as boron and graphite, in a polymeric matrix is one such endeavor. Regardless of whether these composite materials are used exclusively or as selective reinforcement of metallic structures, almost all applications use metal fittings for structural attachments. Providing an efficient load transition from the composite to the metal fitting has been one of the major design problems in the use of composites. To alleviate this problem, a number of different bonded-joint configurations such as lap shear, scarf, and step joints have been proposed (refs. 1, 2, and 3). To design efficient bonded joints, the stresses and strains induced in the joints by applied loads must be known.

The purpose of this investigation was to conduct an experimental and analytical evaluation of a boron-expoxy-reinforced titanium landing-gear drag strut to demonstrate its potential for application to commercial aircraft service. The strut was designed and fabricated by The Boeing Commercial Airplane Company as a company

sponsored program, and the structural evaluation of the strut was conducted at Langley Research Center. The experimental evaluation included both cyclic and static loading. The analytical evaluation involved the use of the NASTRAN® (NASA Structural Analysis) computer program (ref. 4) to compute the stresses and strains in the strut, which are compared with the experimental strains. Results of the evaluation of the bonded joint are presented in reference 5 and are included in this report for completeness.

SYMBOLS

Values are given in both SI and U.S. Customary Units. Measurements and calculations were made in U.S. Customary Units. Factors relating the two systems are given in reference 6.

X	longitudinal axis
Y	transverse axis
x,y	distance along X- and Y-axis, respectively, cm (in.)
σ	axial stress, Pa (psi)
τ	shear stress, Pa (psi)

Superscript:

*	normalizing value

Abbreviation:

SG	strain gage

TEST SPECIMEN

The test specimen was designed to meet the performance specifications of the main body landing gear of a Boeing 747 transport aircraft (fig. 1). The design ultimate loads, calculated critical loads for modes of failure, and margins of safety are given in table I. A shear instability load of 31.96 MN (7185 kips) was calculated for the laminated titanium sheets near the ends of the drag strut by using techniques described in reference 7. Euler and short-column buckling loads were calculated to be 5.08 MN (1141 kips) and 3.14 MN (707 kips), respectively, with equations obtained from reference 8. The weakest part of the strut loaded in tension was the net section at the pinned attachment in the all-titanium end fitting, with a predicted failure load of 2.38 MN (534 kips).

Details of the strut are shown in figures 2(a), 2(b), and 2(c). Except at the ends, where the strut is entirely laminated titanium, unidirectional boron-epoxy is used to stiffen the thin titanium cover skins and provides 80 percent of the load-carrying capabilities of the strut. Figure 2(b) is a cross-sectional view of the I-beam configured strut and shows the boron-epoxy reinforcement at the extremities of the flanges. The remainder of the strut was fabricated of titanium-faced aluminum-honeycomb-core sandwich. No mechanical fasteners were used; the entire strut was adhesively bonded. The total weight of the completed strut is 338 N (76 lbf) and is 30 percent less than the all-titanium production drag strut.

Figure 2(c) shows the details of construction of the strut ends. Each titanium sheet, which has a uniform 0.017 rad (1^{o}) tapered scarf and a 16-ply boron-epoxy laminate in which the plies terminated at 1.02-cm (0.4 in.) steps, were bonded in a cocure process at 450 K (350^{o} F). The boron-epoxy consisted of 0.102-mm-diameter (0.004 in.) filaments embedded in an epoxy matrix with a 50-percent volume fraction. Eight of these straps plus the titanium cover skins were secondarily bonded with AF-126 adhesive cured at 394 K (250^{o} F) to form the load-carrying portion of each of the flanges. The honeycomb core was also bonded in place at the same time. The materials used in the fabrication of the drag strut are listed in table II.

TEST PROCEDURES AND RESULTS

The experimental evaluation of the drag strut was conducted at Langley Research Center. Three different tests were performed on the drag strut: fatigue test, static tension test to the design ultimate load, and static compression test to the design ultimate load. (See fig. 3.) Forty-eight strain gages were bonded to the strut at various locations and were monitored throughout the tests.

Fatigue Test

The drag strut was exposed to two lifetimes of cyclic loading in a 1.78-MN-capacity (400 kips) fatigue test machine. This loading was obtained from The Boeing Company and simulates 0.3g braking loads (assumed to occur an average of five times per flight) experienced during take-off, landing, and taxiing for four types of flights. The four types of flights were training flights, 1-hr flights, 3-hr flights, and 7-hr flights (table III). The highest load in the block, 355 kN (79 800 lbf) in tension, is only 22 percent of the tensile design ultimate load. Each of the four types of flights has distinct mean and alternating loads.

These four different load levels have been randomly arranged in a block of 33 cycles (table IV). This block of loading (33 cycles)

was obtained by dividing the 99 000 cycles per life shown in table III into the smallest block in which all four types of loading would occur at least once. Figure 4 shows a sample of the loading history. This block of loading was applied repeatedly until two lifetimes of loading (198 000 cycles) were accumulated. The cyclic load was applied at a rate of 5 Hz. No hysteresis heating was detected.

The highest load in the block was applied by manual control every 100 blocks of loading for a strain survey. These strain data were monitored for indications of damage which might occur in the strut as a result of the cyclic loading. Samples of these data, shown in figure 5 where strain is plotted as a function of the number of cycles of loading, show no significant change during the test. Strain gage 1 (fig. 2(c)) is located over the first ply of boron-epoxy in the bonded joint, and strain gage 12 (fig. 2(b)) is located over the center portion of the boron-epoxy at the midplane of the strut. The small, random variations in the strains are believed to have been caused by ambient temperature changes during the test. Strain-gage lead wires were temperature compensated, but individual gages were not.

During the fatigue test the drag strut was ultrasonically inspected by using the pulse-echo technique (ref. 9). The strut was monitored at the eight titanium-boron-epoxy joints where the stepped boron-epoxy was one ply thick. No gross changes in ultrasonic damping occurred to indicate bond failure.

At the conclusion of two lifetimes of cyclic loading, the strut was visually and ultrasonically inspected and no damage was detected.

Tensile Test

After the fatigue test was completed, the drag strut was mounted in a 5.34-MN-capacity (1200 kips) static testing machine (fig. 3) and was loaded in tension to the design ultimate load of 1.64 MN (368 kips). Data obtained from strain gages located on the flange at the center of the strut (gages 11, 12, 13, and 14 in fig. 2(b)) indicate that the strut behaved in a linear manner. Maximum strain in this section of the strut was approximately 0.0028 at the tensile design ultimate load.

Similarly, the strain data obtained from the four gages positioned over the first ply of boron-epoxy and 0.51 cm (0.20 in.) from the end of the ply (gages 1, 2, 3, and 4 in fig. 2(c)) indicate that the strains were linear. Maximum strain in this section of the strut was approximately 0.0038 at the tensile design ultimate load.

Strain gages 7, 8, 9, and 10 were positioned on the strut opposite gages 1, 2, 3, and 4, respectively (fig. 2(c)). Because

of the position of a structural spacer, which will be referred to as the end fitting, at the end of the strut, these gages could not be located on the flange. They were located on the tapered portion of the end fitting. Figure 6 is a plot of the strain data obtained from these gages. These data indicate definite nonlinear behavior, which was limited to the end fitting and will be discussed in greater detail in another section of this report.

The strut was visually and ultrasonically inspected before and after the test and no damage due to loading was indicated.

Compression Test

Following the tensile test the strut was mounted in the compression side of the static testing machine (fig. 3) and loaded to the compression design ultimate load of 2.83 MN (636 kips). Figure 7 is a plot of strain-gage data obtained from locations on the flange at the center of the strut (gages 11, 12, 13, and 14 in fig. 2(b)). These data indicate that the strains were linear. Maximum strain in this section of the strut was approximately 0.0051 at the compression design ultimate load.

Figure 8 is a plot of the compression data obtained from strain gages 1, 2, 3, and 4 shown in figure 2(c). Maximum strain at the compression design ultimate load was approximately 0.0060 in this section of the strut. Again, the data indicate that the strut behaved linearly and no apparent damage was detected.

The strain data obtained from gages 7, 8, 9, and 10 (fig. 2(c)) were nonlinear and are presented in figure 9. These gages behaved similarly in both the tension and compression tests. As previously stated, this nonlinearity will be discussed in greater detail in another section of this report.

Similar data were obtained from strain gages at the other end, on the other flange at the center of the strut, and at several locations along the length of the strut. No indication of a buckling condition being approached was detected.

ANALYTICAL EVALUATIONS

Bonded Joint

Finite-element model.- In order to obtain a better understanding of the bonded joint in the drag strut, a two-dimensional finite-element model was developed. Although the bonded joint consisted of 8 titanium straps with 16 plies of boron-epoxy each, it was only necessary to perform an analysis on one (the outermost) strap and the associated face sheet. The model represented the face sheet,

the adhesive layer, the titanium strap with 16 steps, one ply of boron-epoxy bonded to each step, and a second adhesive layer located between the first and second straps (fig. 10). Even though the titanium strap had a uniform scarf, it was modeled as a uniformly stepped joint since each ply of boron-epoxy in the drag strut ended in a discrete step. Each ply of boron-epoxy was divided into equal volumes of boron and epoxy. The boron filament volume was assumed to be distributed in a continuous, uniform layer sandwiched between equal volumes of epoxy. Nominal material properties were assumed and are listed in table V.

The parameters computed in this study consisted of the shear and normal stresses, forces at the constrained grid points, and displacements of the grid points. The boundary conditions for the model consisted of the following:

(1) A constraint on the displacements at $x = 0$ (fig. 10)

(2) A constraint on the row of grid points between plies 7 and 8, allowing no motion in the y-direction

(3) A uniform extension (strain which corresponds to the design ultimate load) in the x-direction applied to the right edge ($x = 21.3$ cm (8.4 in.)) of the joint model

Analytical results.- Shear stress data obtained from the finite-element model are presented in figure 11, where the normalized shear stress is plotted as a function of position along the joint model. The curve shows the shear stress pattern of the row of elements containing the upper epoxy matrix of the first ply of boron-epoxy. This row of elements was found to be the most highly stressed in the joint. At the left edge of the model, the shear stress is zero in the titanium strap. The stress remains small until the first step, at which point the peak stress (70.3 MPa (10.2 ksi)) in the titanium occurs. The next element, which is the first element of epoxy, has a considerably lower stress value of 26.1 MPa (3.78 ksi), but the peak matrix shear stress (37.5 MPa (5.44 ksi)) occurs in the second epoxy element. This peak matrix shear stress is approximately 50 percent of the matrix material shear strength (ref. 1). The shear stresses for the second and third steps are considerably lower than that for the first step. From this point to the right edge of the joint model, the shear stress is small (essentially zero) with negligible perturbations at subsequent steps.

By combining similar data for each of the 16 plies of boron-epoxy, a shear stress distribution through the length of the joint was obtained (fig. 12). The curve in figure 12 is faired through the peak shear stress in the matrix of each ply. The stress in the second ply is considerably lower than that in the first ply, and the stress in each successive ply is less than that in the preceding ply throughout the joint to the end of the titanium strap. An

abrupt change in the shear stress is associated with the end of the strap. This peak stress is approximately 0.59 of that in the first ply. Beyond the end of the titanium strap there are no further changes in material, and the shear stress is zero at the end of the joint model.

In figure 13 the normalized axial stress of the first ply of boron is plotted as a function of distance along the model. In the vicinity of the first step the stress is relatively high. At the second step the stress is greater than that at the first step; this is the location of maximum fiber axial stress (1420 MPa (206 ksi)). At this location there is only matrix material which bonds the end of the second-ply fiber to the titanium. The modulus of the matrix is significantly less than that of either the boron fiber or the titanium; therefore, an insignificant tensile load is transmitted across this region. This load is transmitted through shear to the boron in the first ply. The perturbation in the axial stress is lower at each successive step. There are no further changes in configuration from the end of the strap to the end of the model and the axial stress is constant at 0.62 of the peak stress.

The analysis shows that the largest shear stresses induced in the critical matrix areas during the static tensile loading are about half of the matrix material strength. Thus, for static tensile loads, the bonded joint is less critical than the all-titanium net section at the pinned ends. Because the peak fatigue loads are only 22 percent of the design ultimate load, the cyclic shear stresses in the matrix are only about 10 percent of the matrix strength; therefore, a long life is to be expected. The bonded-joint fatigue data in reference 10 indicate that, at the load levels in the drag-strut fatigue spectrum, the bonded joints would survive at least 10 times the number of cycles the strut was exposed to.

In order to verify the analysis of the joint, computed strains were compared with experimental values. This comparison is presented in figure 14 where the applied load is plotted as a function of the measured strain. The solid lines are the experimental data obtained from strain gages during static loading to the tensile design ultimate load (1.64 MN (368 kips)). The symbols represent computed values of strain at model locations that correspond to the specified strain-gage locations. At the tensile design ultimate load, the agreement is excellent at the all-titanium area (gage 5), at the first ply of boron-epoxy (gage 1), and at the area beyond the joint in the all-boron-epoxy area (gage 6).

End Fitting

The strain-gage data indicate inelastic and creep behavior at the end fitting (figs. 6 and 9). This behavior was hypothesized to

be a result of the inelastic adhesive. Thus, a nonlinear finite-element analysis of this area was performed.

Finite-element model.- This model was developed to analyze the nonlinear behavior of the tapered end fitting. Figure 15 shows the model, including portions of the flange, the adhesive layer, and the tapered end fitting. The boundary conditions for the model consisted of the following:

(1) A constraint on the displacement in the x-direction at $x = 0$ (fig. 15)

(2) A constraint on the displacement in the y-direction at $y = 0$ to eliminate bending

(3) A uniformly distributed load (tensile design ultimate load) applied in the x-direction at $x = 14.0$ cm (5.5 in.)

The parameters computed consisted of shear and normal stresses, forces at the constrained grid points, and displacements of the grid points. These parameters were initially computed for elastic adhesive properties. They were then computed for inelastic mechanical properties for 10 of the adhesive elements (fig. 15). Figure 16 is a plot of the assumed stress-strain data used to compute the parameters for the inelastic adhesive.

Analytical results.- For the design loads, only a small portion of the adhesive was considered to be inelastic. Only the 10 elements shaded in figure 15 were given inelastic mechanical properties in the analysis. Shear stress in the elements beyond the first 10 was sufficiently low to be within the first segment of the stress-strain curve (fig. 16). Figure 17 is a plot of the normalized shear stress in the adhesive as a function of location along the model. The data show that the stress in the adhesive was sufficient to cause inelastic behavior.

In order to relate the computed strains in the end fitting to the drag-strut loading, the constrained grid point forces were used to obtain the applied load. These results are shown in figure 18, where the applied load is plotted as a function of strain. The two solid straight lines represent computed results and show the axial strain on the end of the end fitting (corresponding to the location of strain gages 7, 8, 9, and 10 in figs. 2(c), 6, and 9) for purely elastic adhesive and inelastic adhesive. The inelastic adhesive has a significant effect on the strain response of the end fitting, as shown in figure 18. Since time-dependent material behavior is not included in the computer program, the incorporation of creep (time dependency) into the analysis was not possible. Therefore, the nonlinear load-strain curves shown in figures 6 and 9 could not be duplicated analytically. If this could be done, however, a curve would be obtained which would be similar to the dashed curve shown in figure 18. This curve shows a reduced strain in the titanium end

fitting due to creep of the adhesive (ref. 11). Creep was evident in the experimental data where the strain in the fitting decreased while maximum load was momentarily held on the strut (figs. 6 and 9).

SUMMARY OF RESULTS

Structural performance has been evaluated experimentally and analytically on a boron-epoxy-reinforced titanium drag strut containing bonded scarf joints. Weight savings of 30 percent over existing all-metal components have been achieved in a fabricated part that was designed with conservative margins of safety. The results of this investigation are summarized as follows:

1. The drag strut was exposed to two lifetimes of fatigue loading and loaded in tension and compression to the respective design ultimate loads without the occurrence of any detectable damage.

2. The analytical study indicated that the peak shear stresses in the bonded joints were sufficiently low to preclude drag-strut failure by disbonding of the joints due to fatigue loading.

3. The analytical study indicated that the peak shear stresses in the bonded joints were sufficiently low to preclude drag-strut failure by disbonding of the joints due to static loading.

4. The analytical study indicated that the nonlinear behavior in the structural spacer at each end of the strut could be explained by the inelastic behavior and possible creep of the adhesive.

Langley Research Center
National Aeronautics and Space Administration
Hampton, VA 23665
September 16, 1976

REFERENCES

1. Oken, S.; and June, R. R.: Analytical and Experimental Investigation of Aircraft Metal Structures Reinforced With Filamentary Composites. Phase I - Concept Development and Feasibility. NASA CR-1859, 1971.

2. Corvelli, Nicholas; and Carri, Robert: Evaluation of a Boron-Epoxy-Reinforced Titanium Tubular Truss for Application to a Space Shuttle Booster Thrust Structure. NASA TN D-6778, 1972.

3. Hart-Smith, L. J.: Analysis and Design of Advanced Composite Bonded Joints. NASA CR-2218, 1974.

4. McCormick, Caleb W., ed.: The NASTRAN User's Manual (Level 15). NASA SP-222(01), 1972.

5. Howell, William E.: Bonded Composite-to-Metal Scarf Joint Performance in an Aircraft Landing Gear Drag Strut. NASA TM X-71995, 1974.

6. Metric Practice Guide. E 380-72, American Soc. Testing & Mater., June 1972.

7. Davis, John G., Jr.: Compressive Strength of Lamina Reinforced and Fiber Reinforced Composite Materials. Ph. D. Thesis, Virginia Polytech. & State Univ., 1973.

8. Timoshenko, Stephen P.; and Gere, James M.: Theory of Elastic Stability. Second ed. McGraw-Hill Book Co., Inc., c.1961.

9. McMaster, Robert C., ed.: Nondestructive Testing Handbook. Vol. II. Ronald Press Co., 1963.

10. Blichfeldt, B.; and McCarty, J. E.: Analytical and Experimental Investigation of Aircraft Metal Structures Reinforced With Filamentary Composites. Phase II - Structural Fatigue, Thermal Cycling, Creep, and Residual Strength. NASA CR-2039, 1972.

11. Christensen, R. M.: Theory of Viscoelasticity - An Introduction. Academic Press, Inc., 1971.

TABLE I.- DESIGN STATIC LOADS AND CALCULATED CRITICAL LOADS

Mode of failure	Design static ultimate load, MN (kips) (a)	Calculated load, MN (kips)	Margin of safety
Compression	2.83 (636)		
Euler buckling		5.08 (1141)	0.80
Short-column buckling		3.14 (707)	.11
Shear instability (titanium sheets at strut ends)		31.96 (7185)	10.29
Tension	1.64 (368)		
Net section at pinned end		2.38 (534)	.45
Joint		2.98 (670)	.82
Center		4.53 (1018)	1.76

[a]These loads are based on a design condition for a 12° tail-down landing plus springback and an ultimate-to-limit factor of safety of 1.5.

TABLE II.- MATERIALS USED IN STRUT

Constituent	Material
Titanium	Ti-6Al-4V
Boron	0.010-cm-diameter (0.004 in.) filaments of boron, vapor deposited onto a tungsten-wire substrate
Matrix	BP-907 epoxy
Adhesive	AF-126

TABLE III.- DESIGN FATIGUE LOADING FOR ONE LIFETIME

Type of flight	Number of cycles (a)	Load level, kN (kips)
1 hr	48 000	45.82 ± 229.53 (10.3 ± 51.6)
3 hr	24 000	49.82 ± 251.77 (11.2 ± 56.6)
7 hr	24 000	62.27 ± 292.69 (14.0 ± 65.8)
Training	3 000	42.26 ± 211.29 (9.5 ± 47.5)

[a]Total of 99 000 cycles per lifetime at 0.3g braking.

TABLE IV.- FATIGUE LOADING BLOCK

Cycle	Type of flight
1	1 hr
2	7 hr
3	7 hr
4	1 hr
5	1 hr
6	7 hr
7	3 hr
8	1 hr
9	7 hr
10	1 hr
11	3 hr
12	1 hr
13	1 hr
14	7 hr
15	1 hr
16	1 hr
17	3 hr
18	3 hr
19	3 hr
20	1 hr
21	Training
22	7 hr
23	1 hr
24	1 hr
25	3 hr
26	1 hr
27	7 hr
28	1 hr
29	1 hr
30	1 hr
31	7 hr
32	3 hr
33	3 hr

TABLE V.- NOMINAL MATERIAL PROPERTIES USED

IN ANALYTICAL STUDIES

Material	Modulus, MPa (psi)		Poisson's ratio
	Young's	Shear	
Titanium	110 316 (16.0×10^6)	42 403 (6.15×10^6)	0.3
AF-126 adhesive	1 517 (220 000)	370 (53 600)	.4
BP-907 matrix	3 103 (450 000)	1 193 (173 000)	.3
Boron	344 738 (50.0×10^6)	142 032 (20.6×10^6)	.2

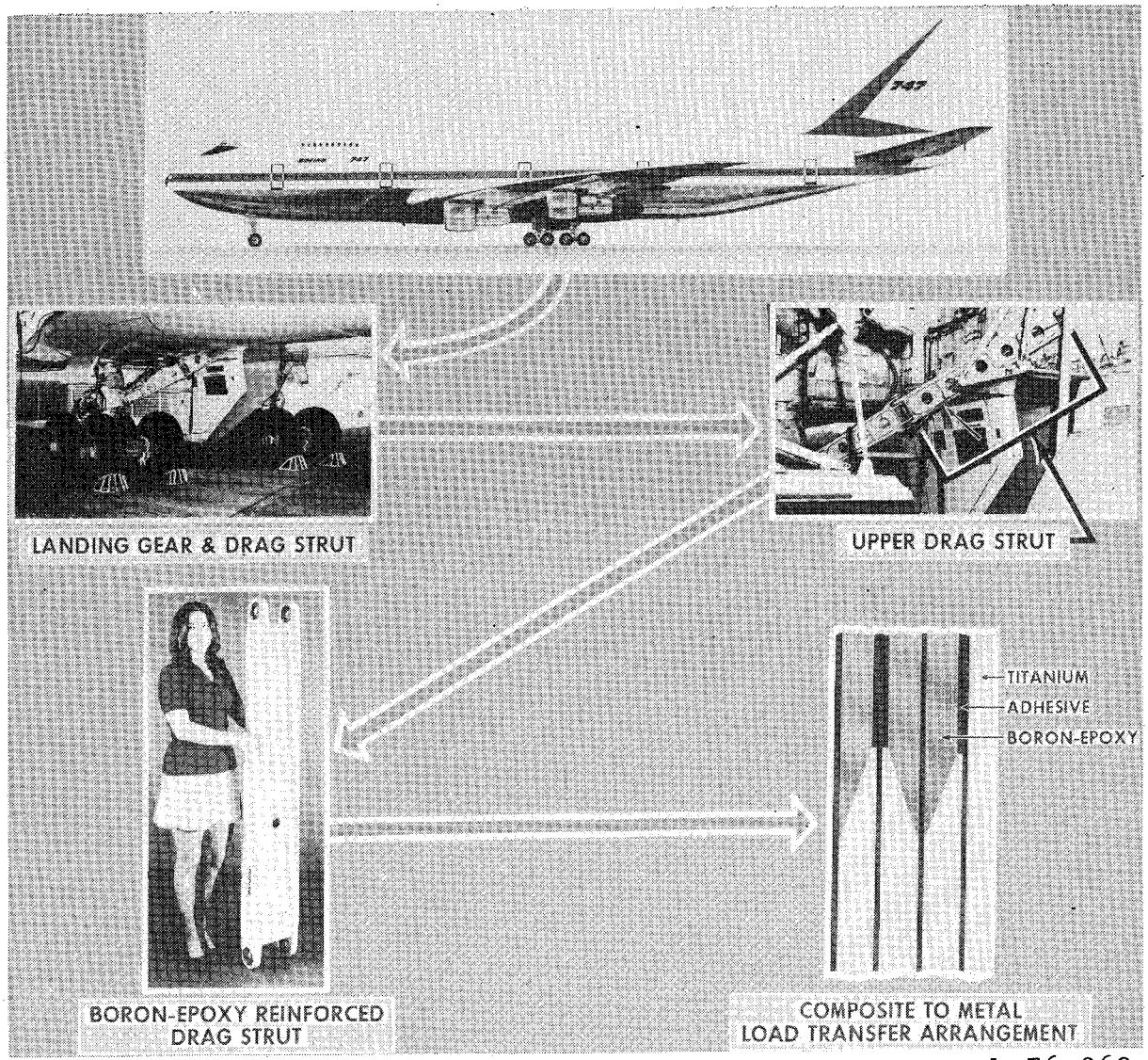

L-76-262

Figure 1.- Composite-reinforced drag strut for Boeing 747 transport.

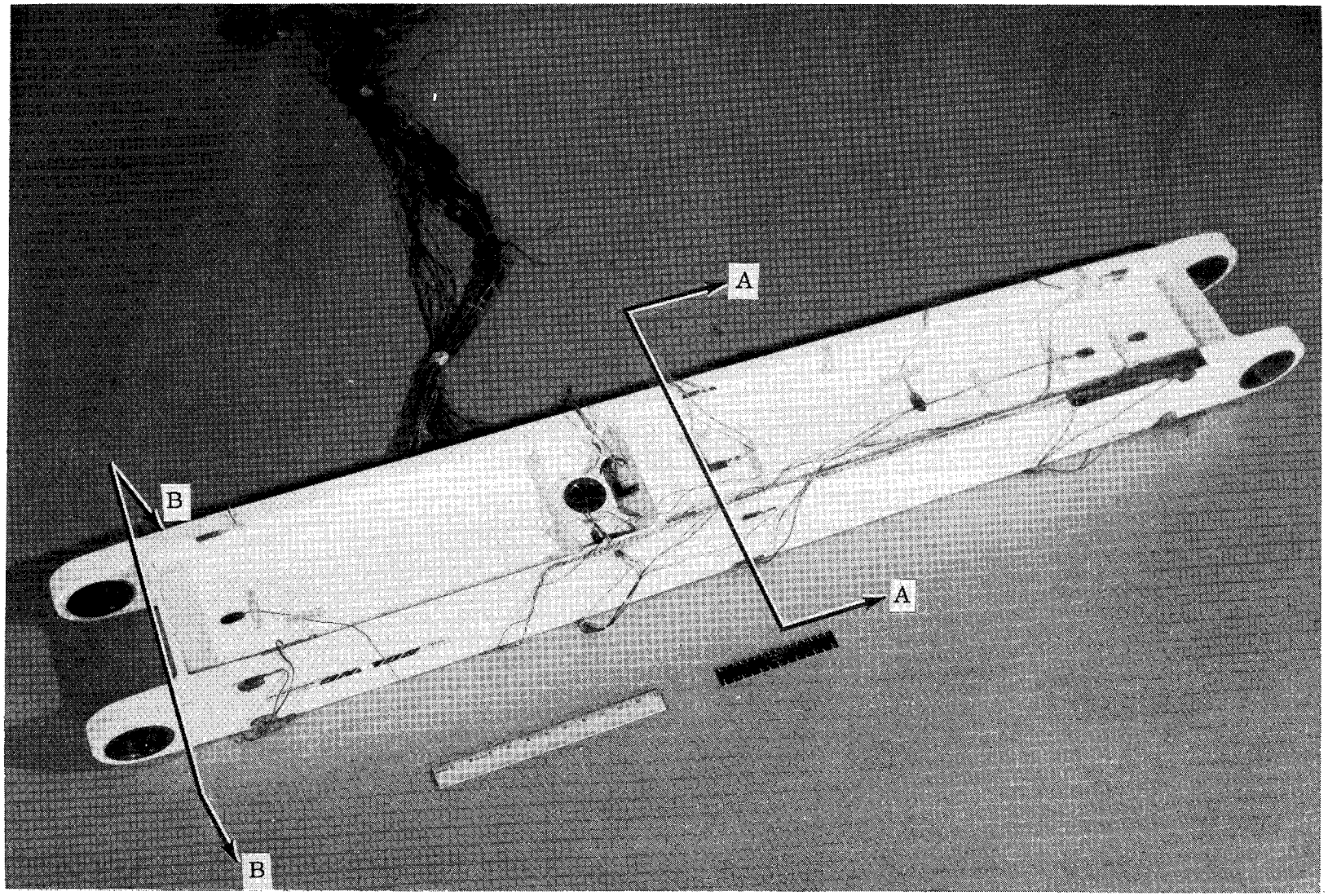

L-74-4088.1

(a) Overall view of drag strut showing locations of view A-A (fig. 2(b)) and section B-B (fig. 2(c)).

Figure 2.- Details of drag strut.

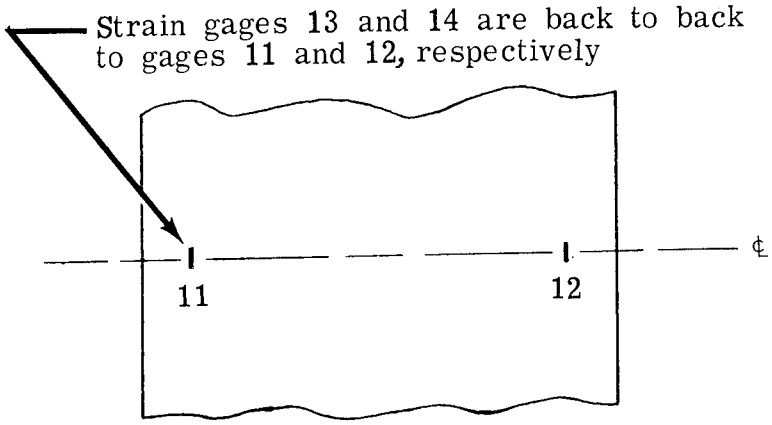

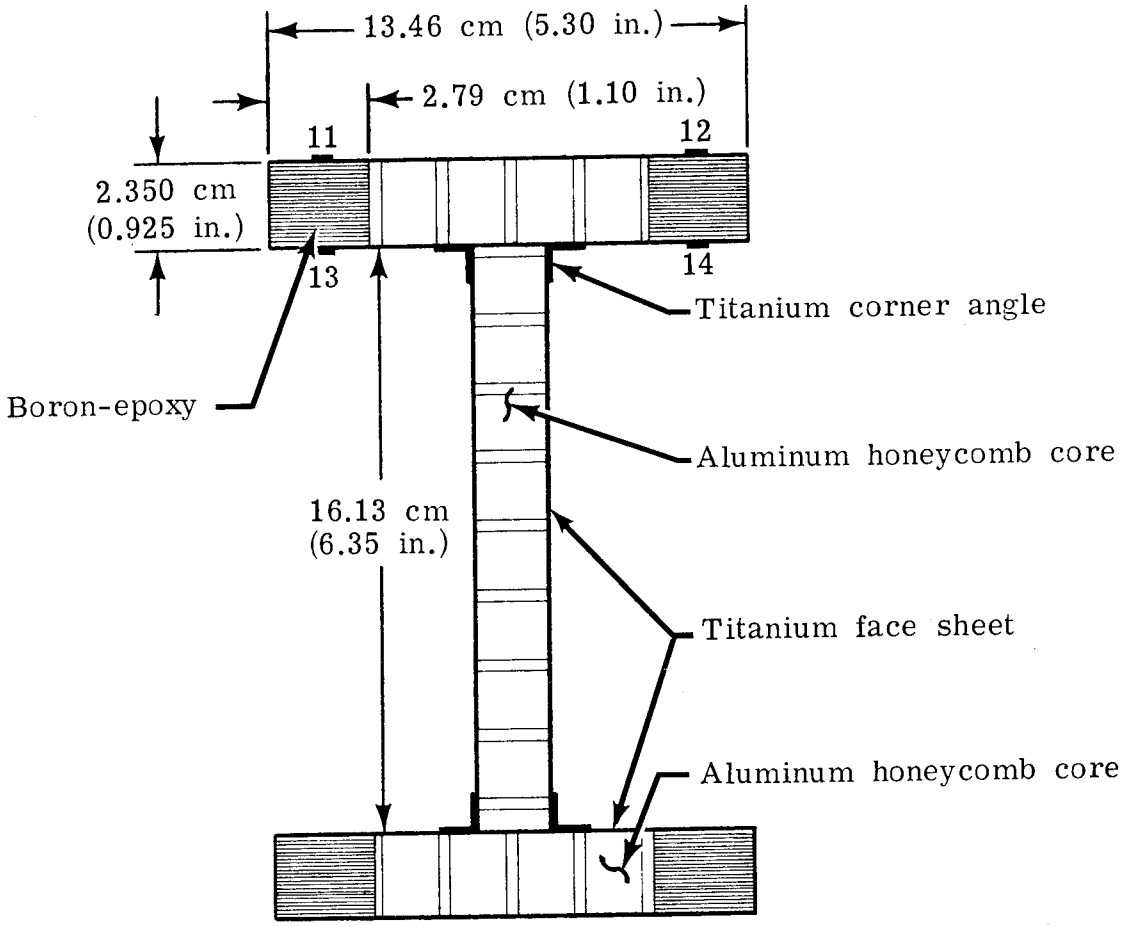

(b) Drag strut cross section at section A-A.

Figure 2.- Continued.

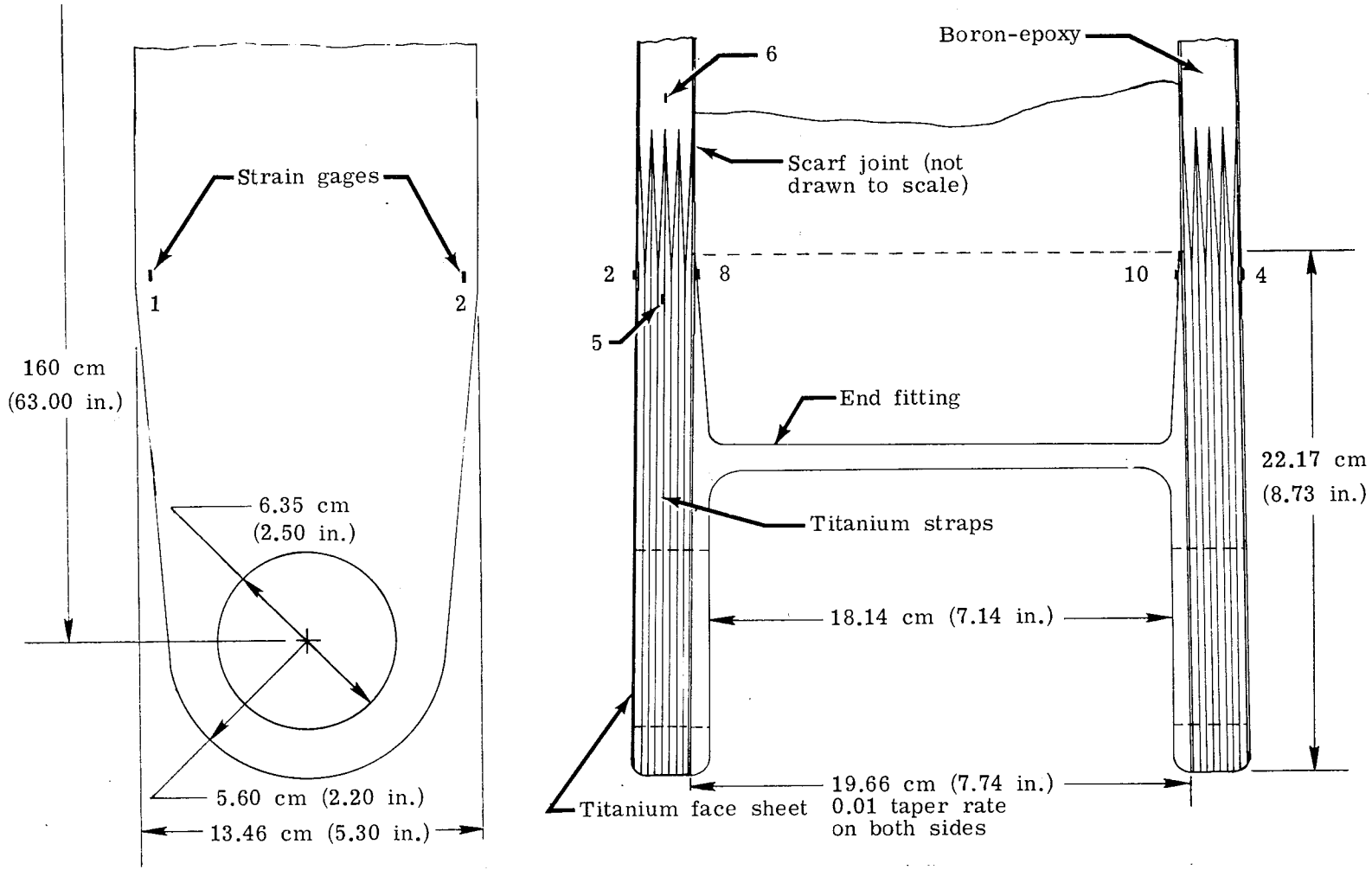

(c) Strain-gage location at boron-epoxy-titanium joints near ends of strut and general arrangement of drag strut ends at section B-B.

Figure 2.- Concluded.

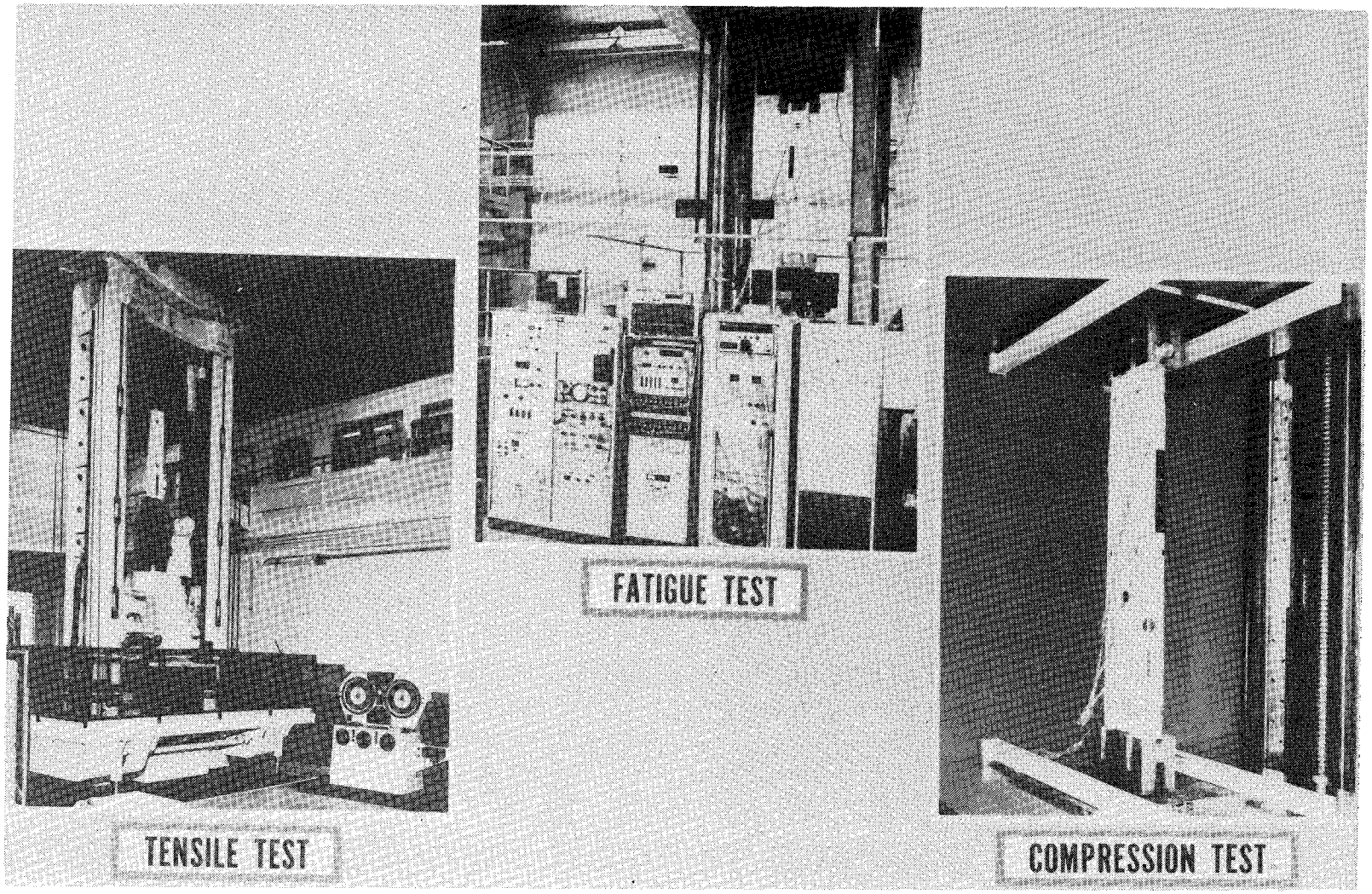

L-76-263

Figure 3.- Experimental test arrangements for composite-reinforced drag strut.

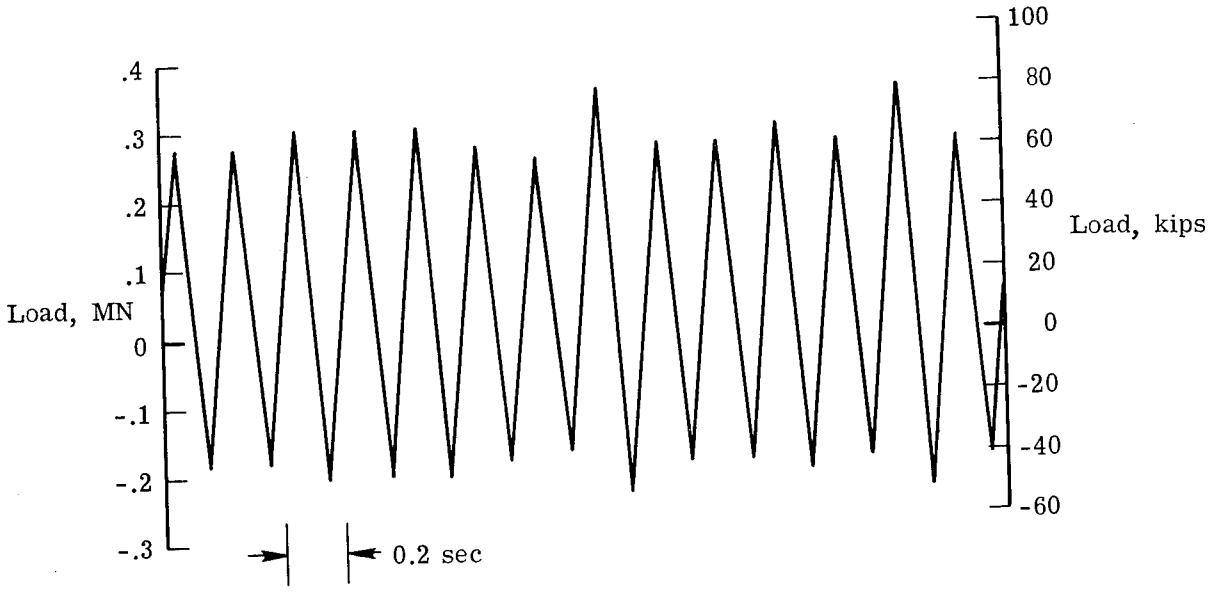

Figure 4.- Sample of fatigue loading.

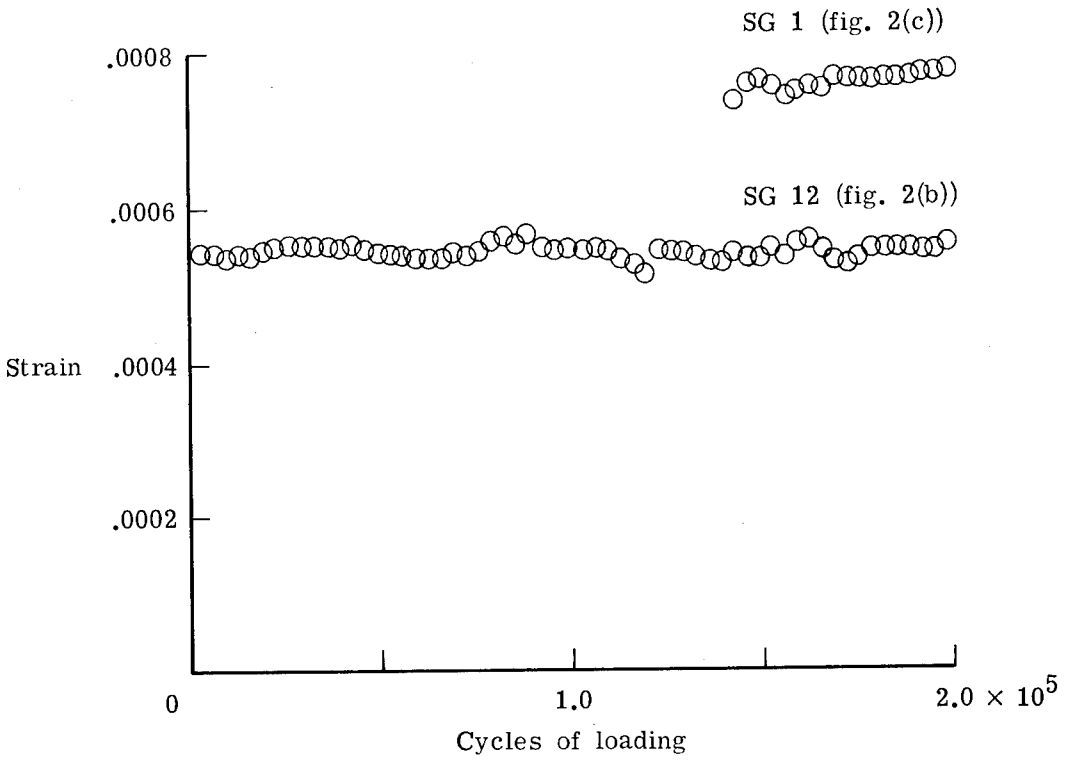

Figure 5.- Strain-gage data from fatigue test. Strains were recorded during a strain survey taken once every 3300 load cycles.

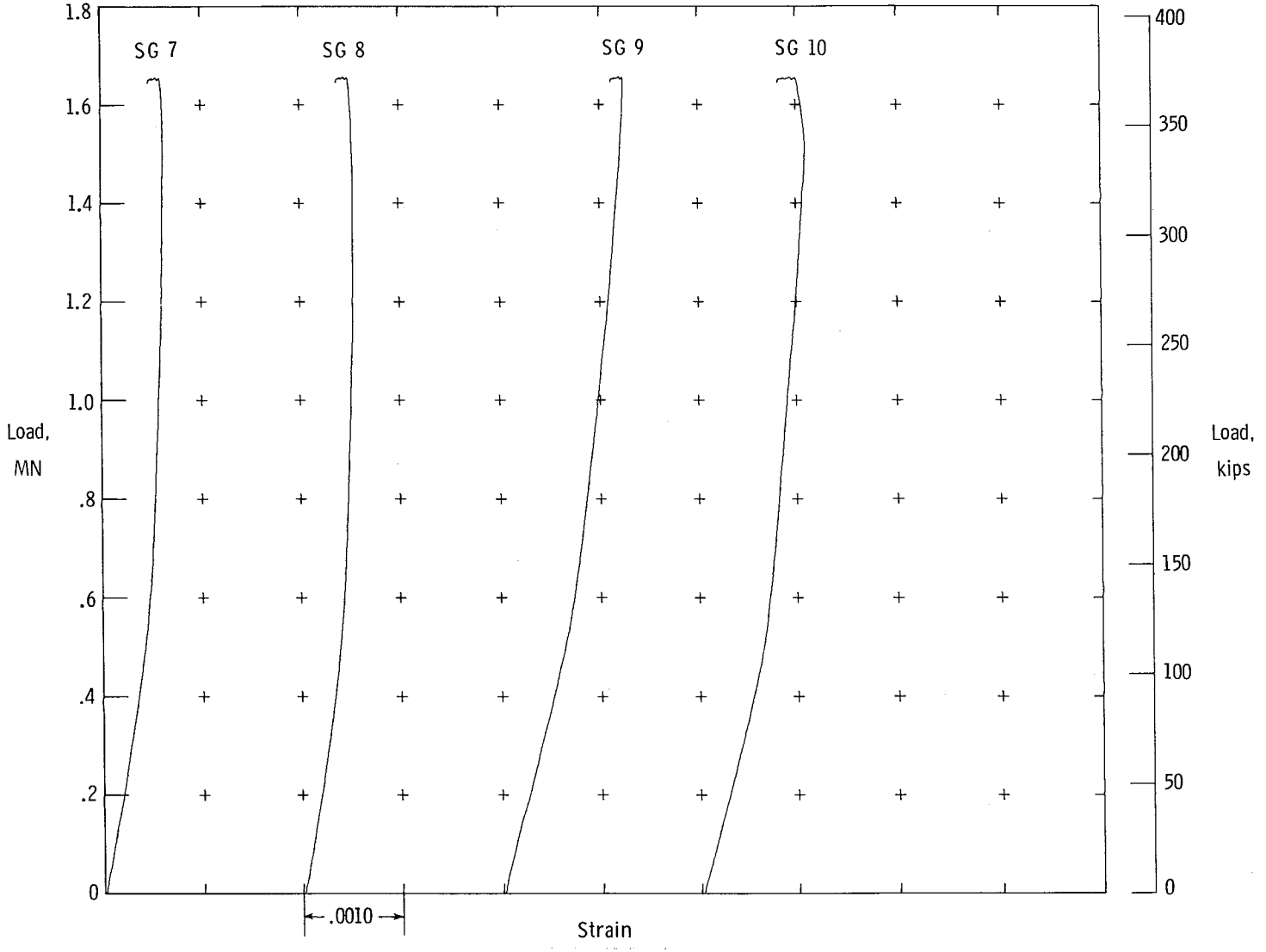

Figure 6.- Strain-gage data for tensile design ultimate load (1.64 MN (368 kips)).

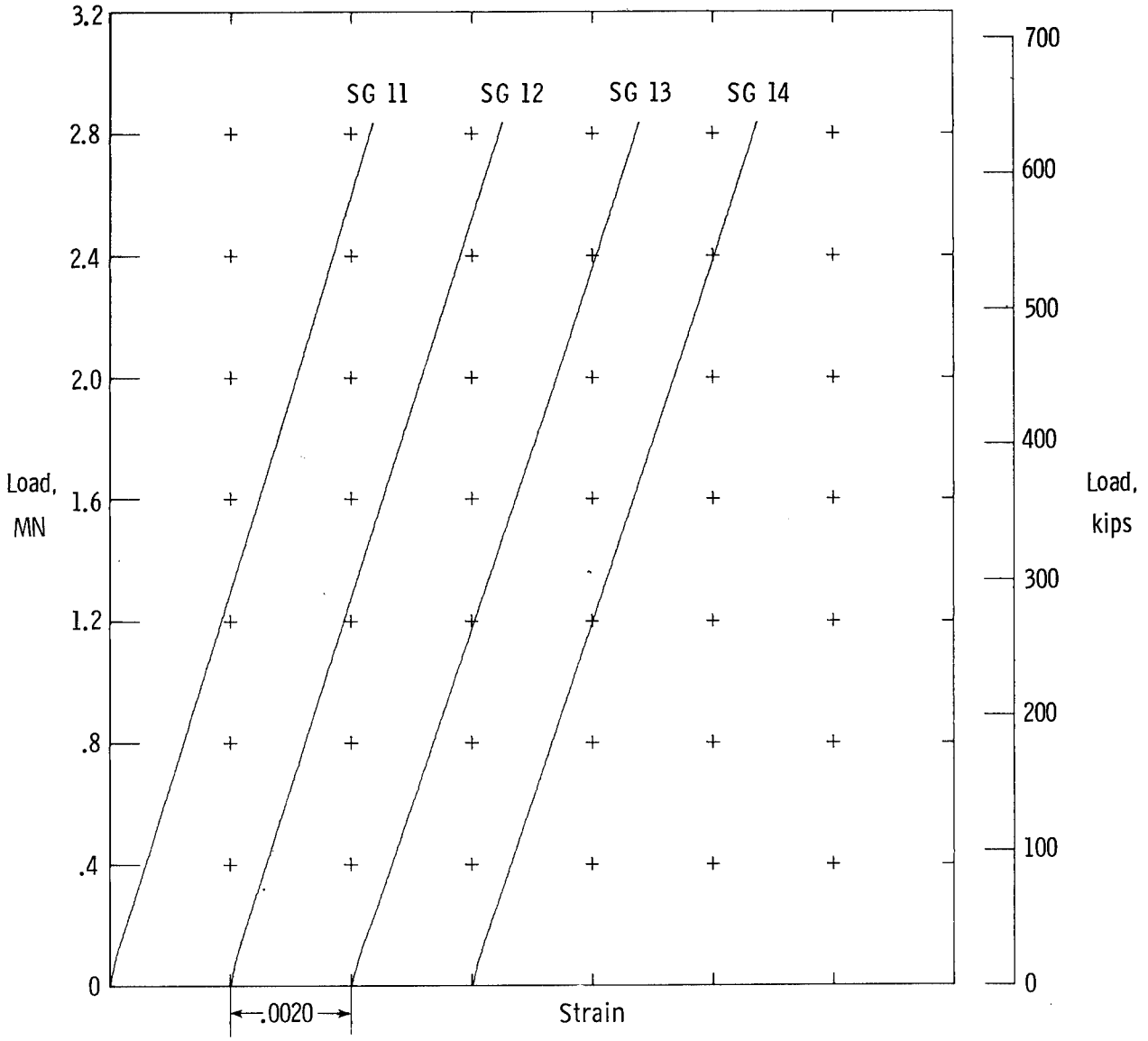

Figure 7.- Strain-gage data for compression design ultimate load (2.83 MN (636 kips)) for strain gages 11 to 14.

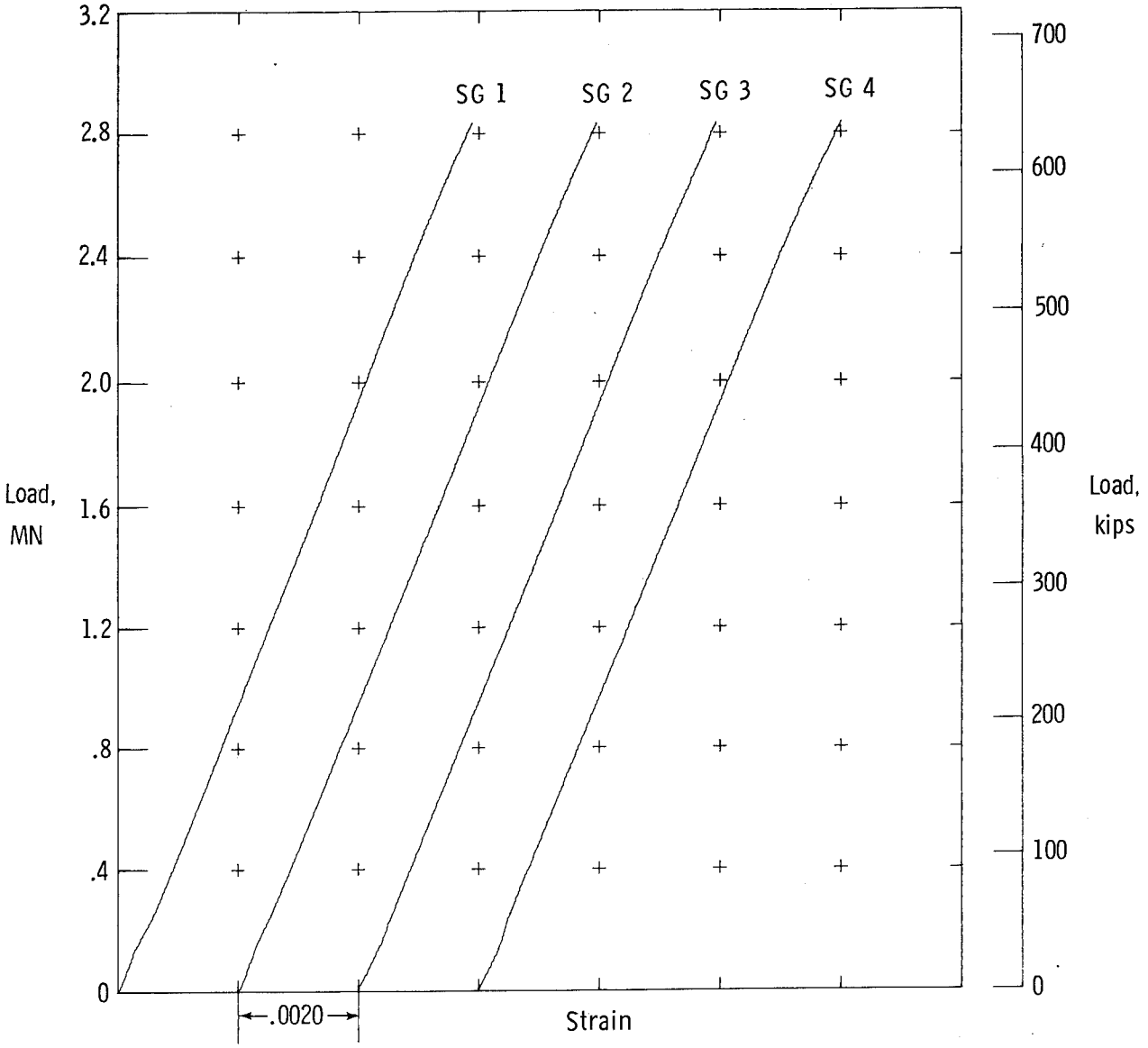

Figure 8.- Strain-gage data for compression design ultimate load (2.83 MN (636 kips)) for strain gages 1 to 4.

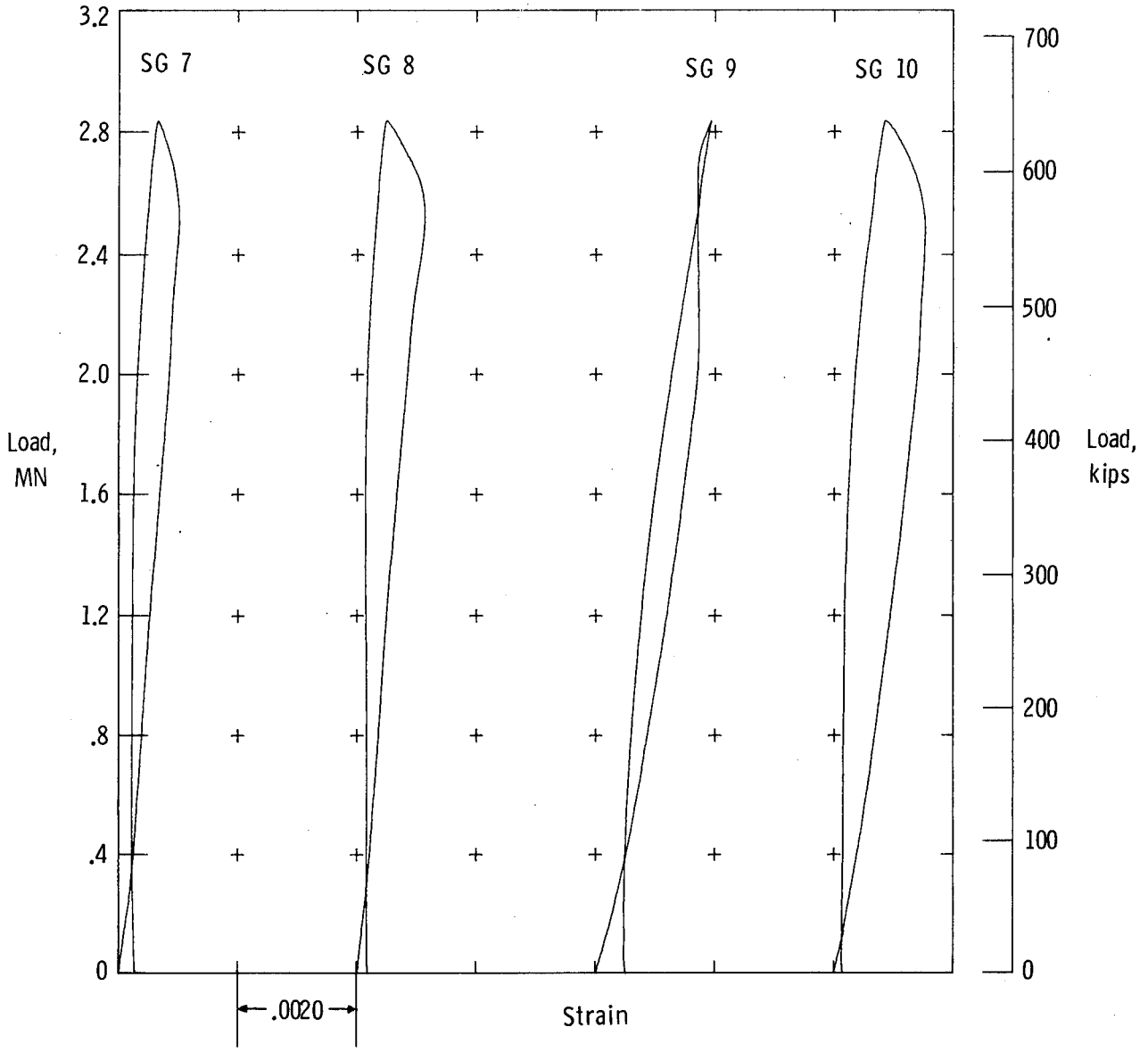

Figure 9.- Strain-gage data for compression design ultimate load (2.83 MN (636 kips)) for strain gages 7 to 10.

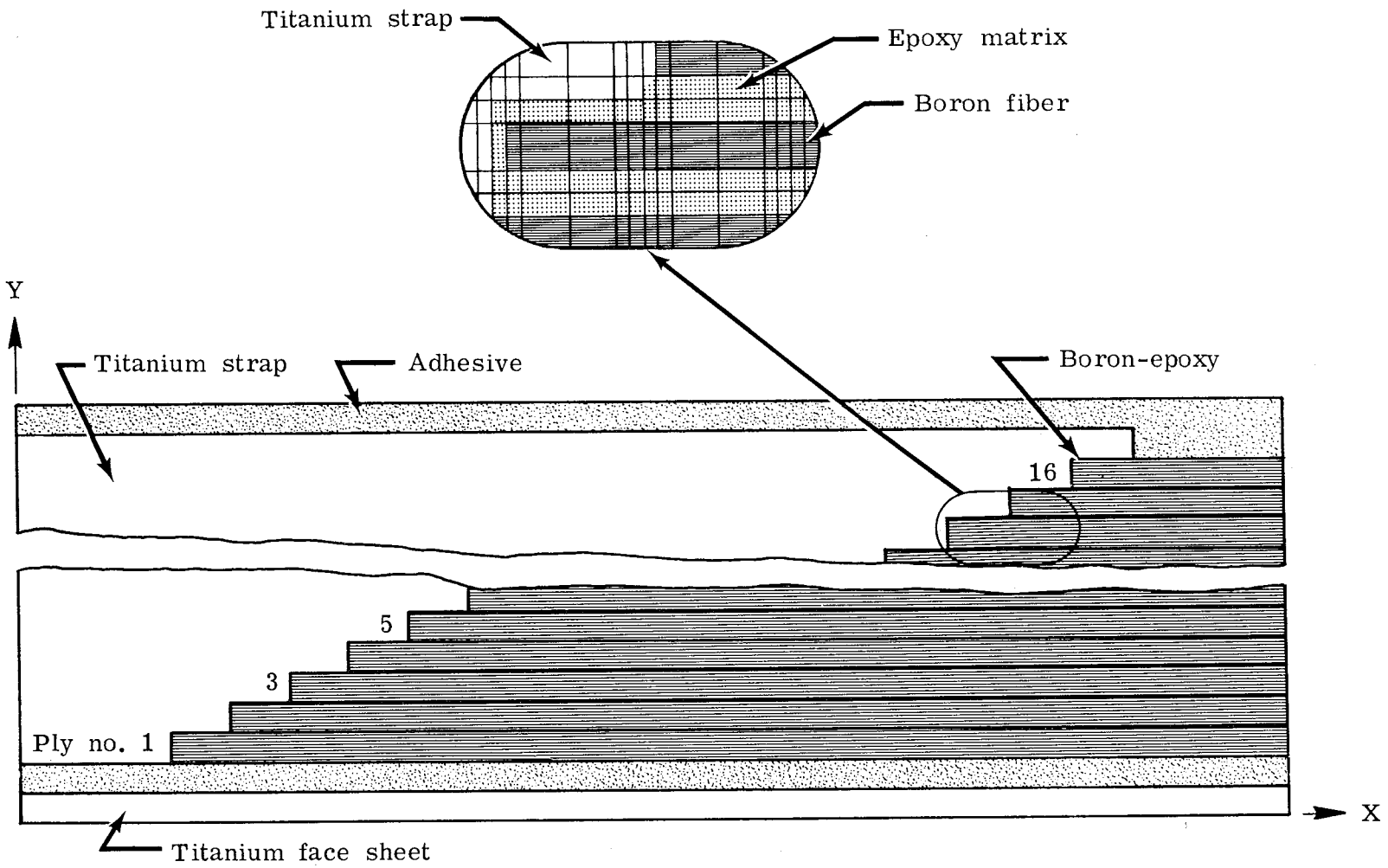

Figure 10.- Structural model used for analytical (NASTRAN®) study.

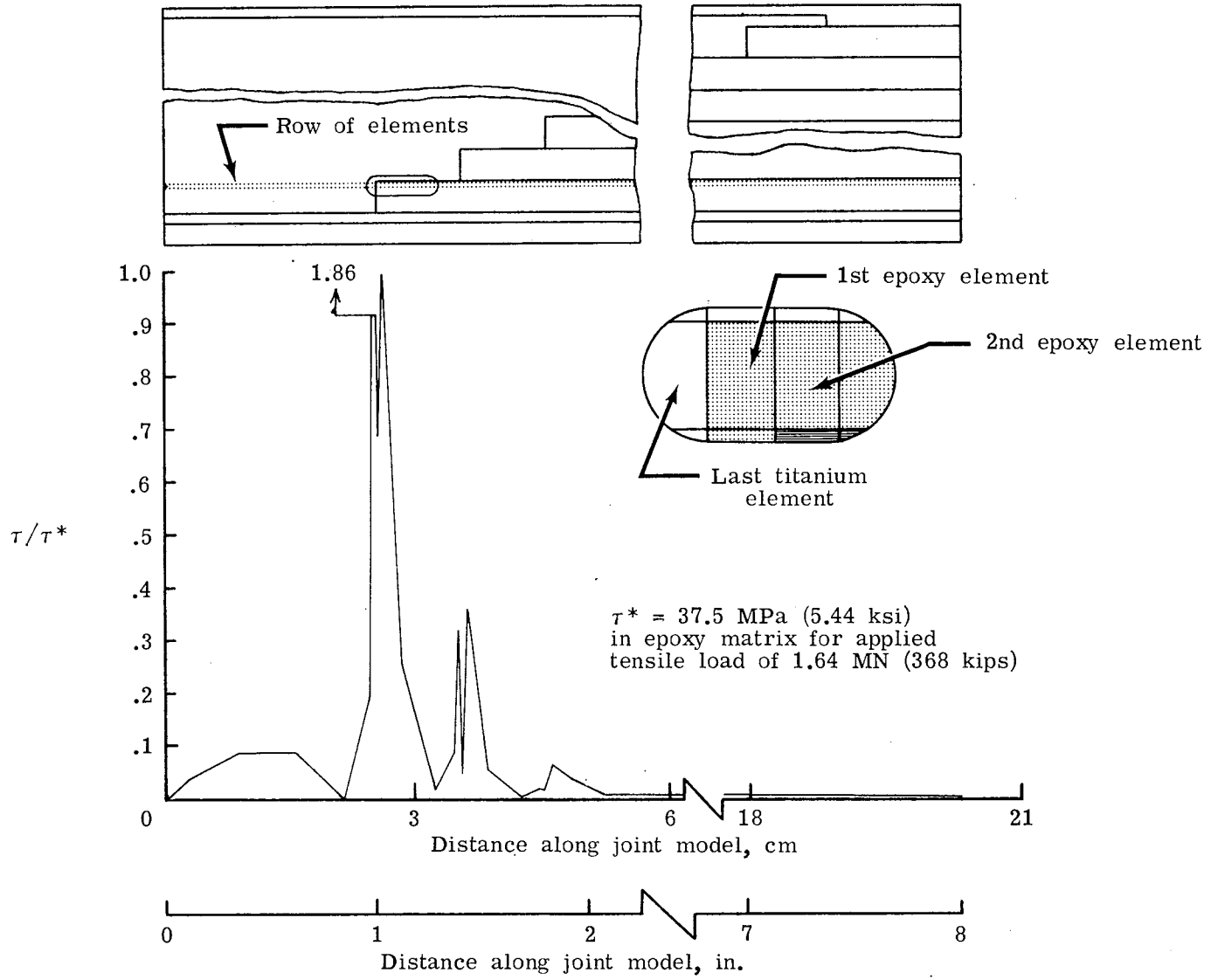

Figure 11.- Shear stress pattern of row of elements containing epoxy matrix of first ply of boron-epoxy.

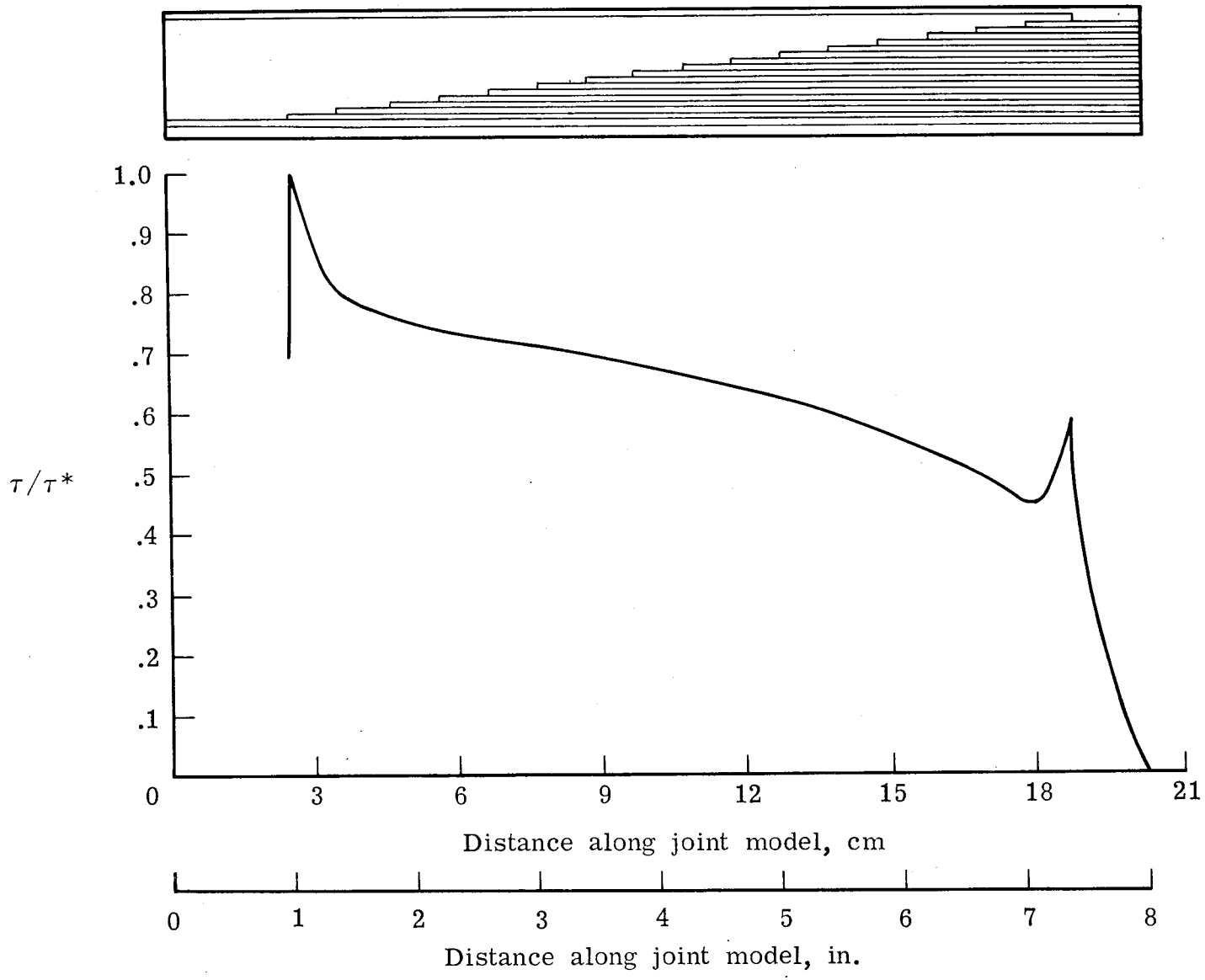

Figure 12.- Peak shear stress distribution along joint.

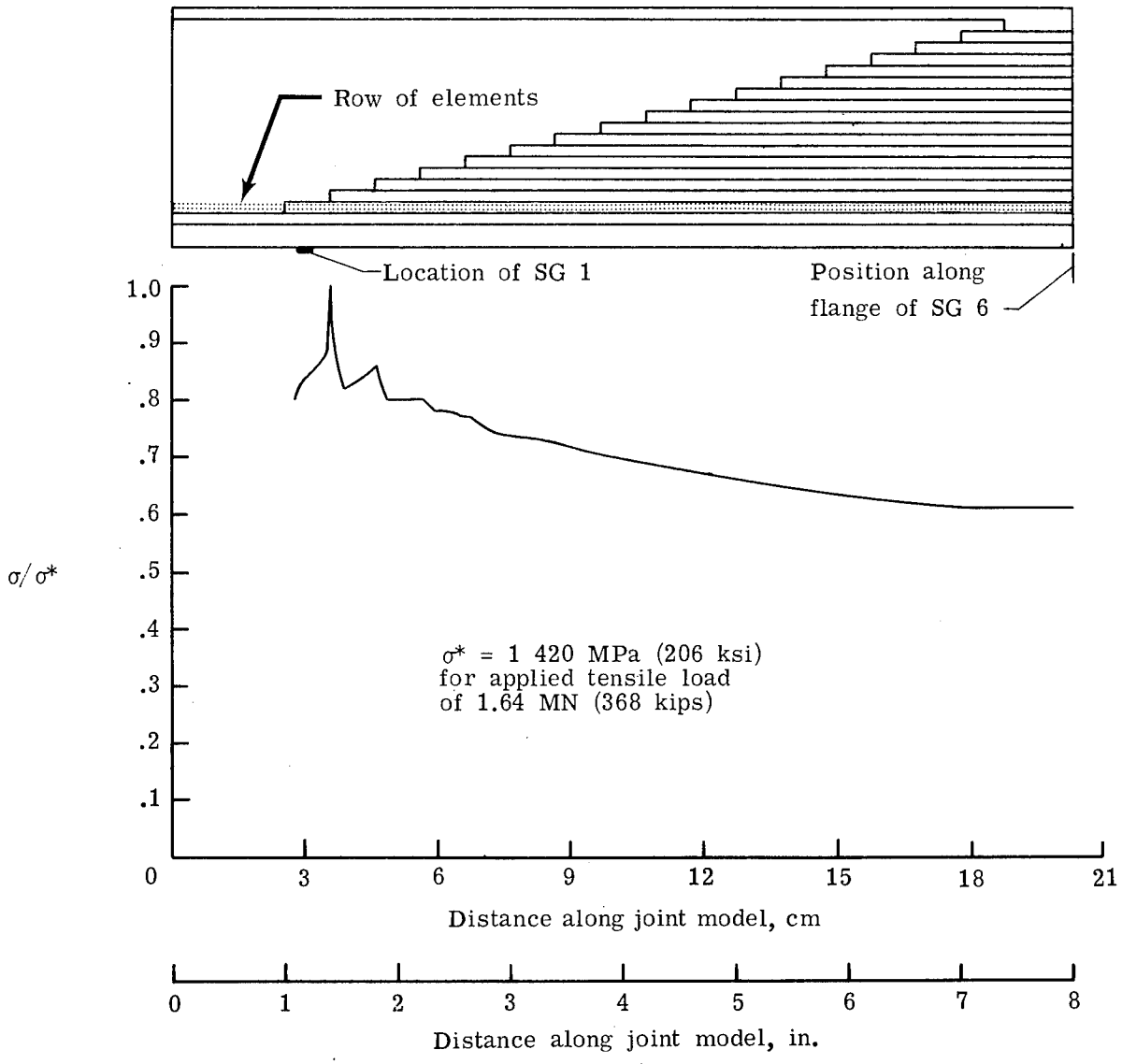

Figure 13.- Axial stress in first ply of boron fibers.

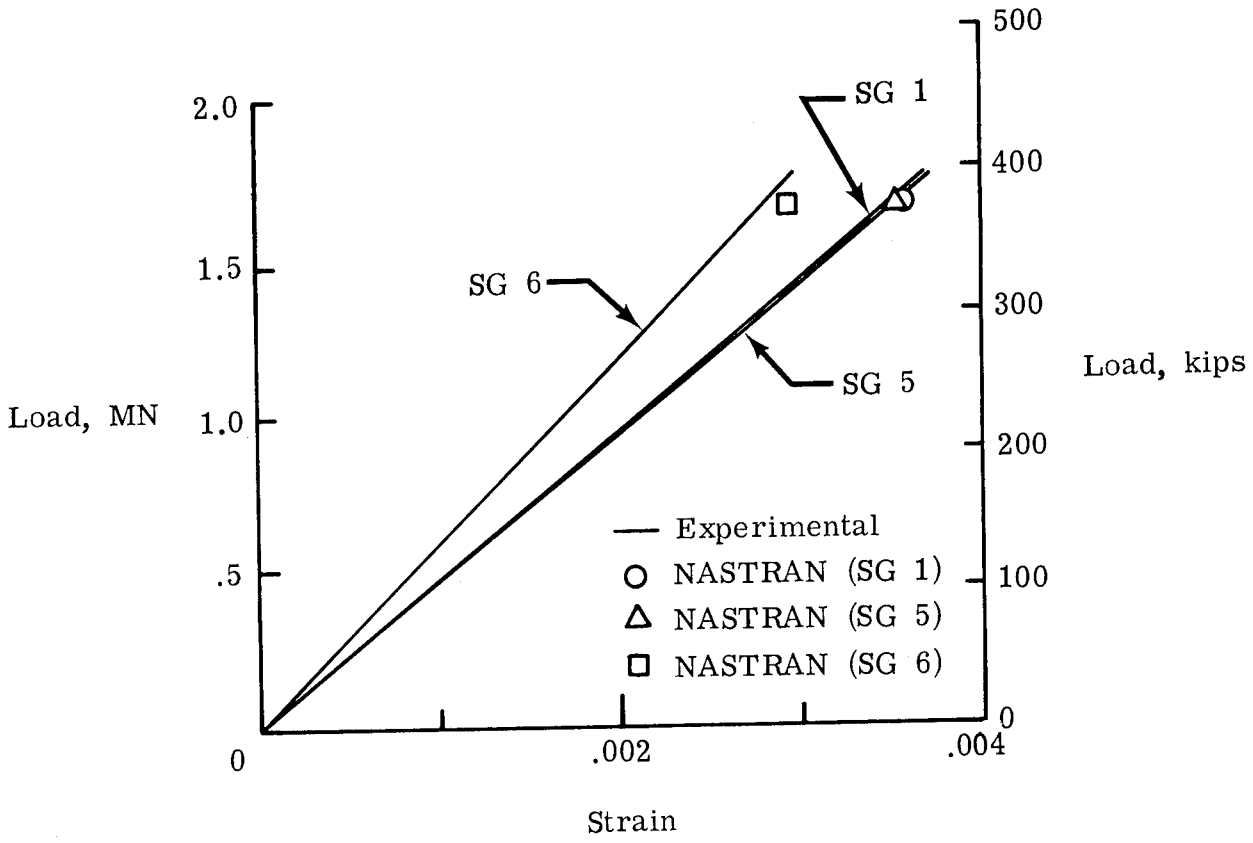

Figure 14.- Comparison of experimentally and analytically (NASTRAN®) determined strains.

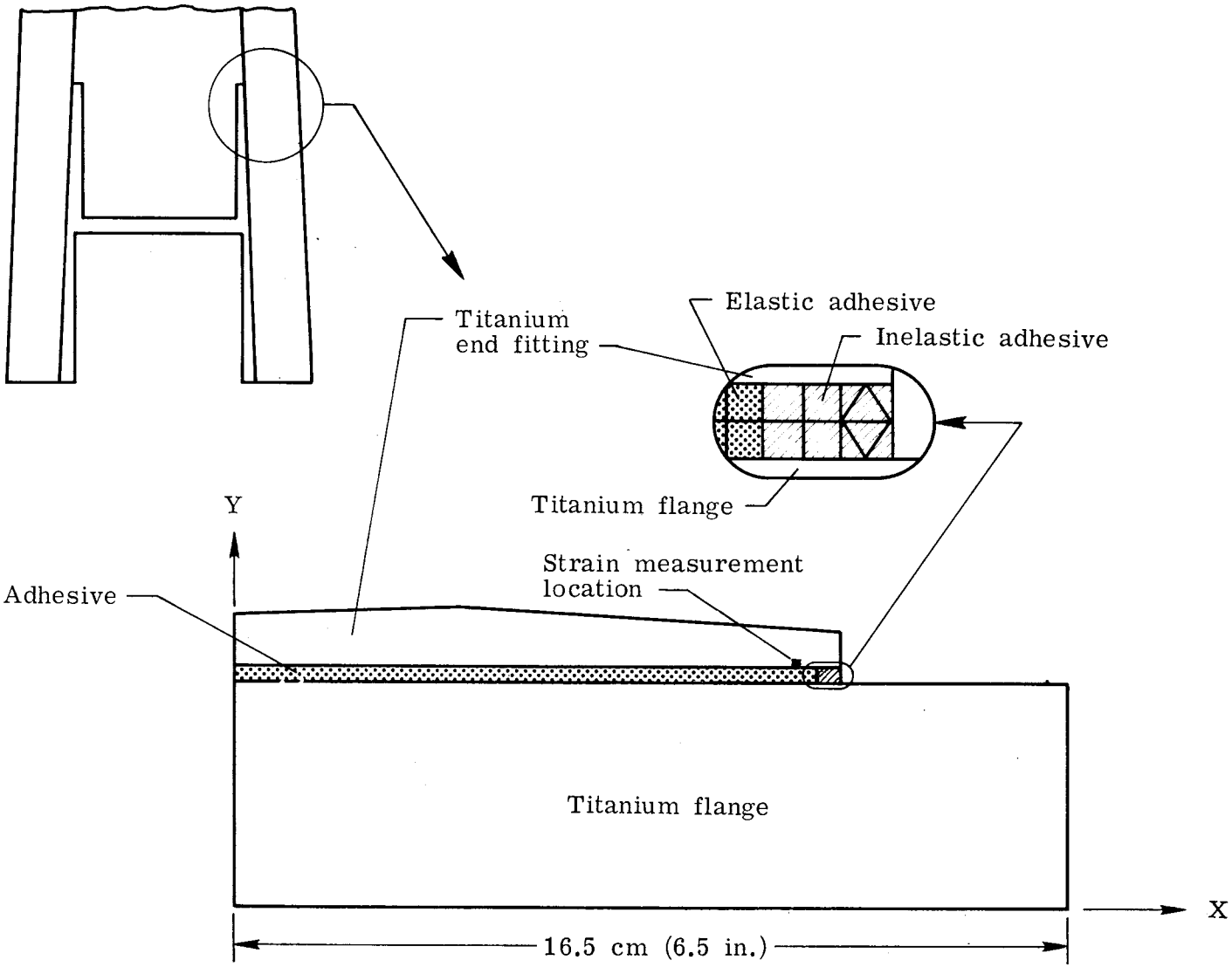

Figure 15.- Model used to evaluate effect of inelastic adhesive on strain of end fitting.

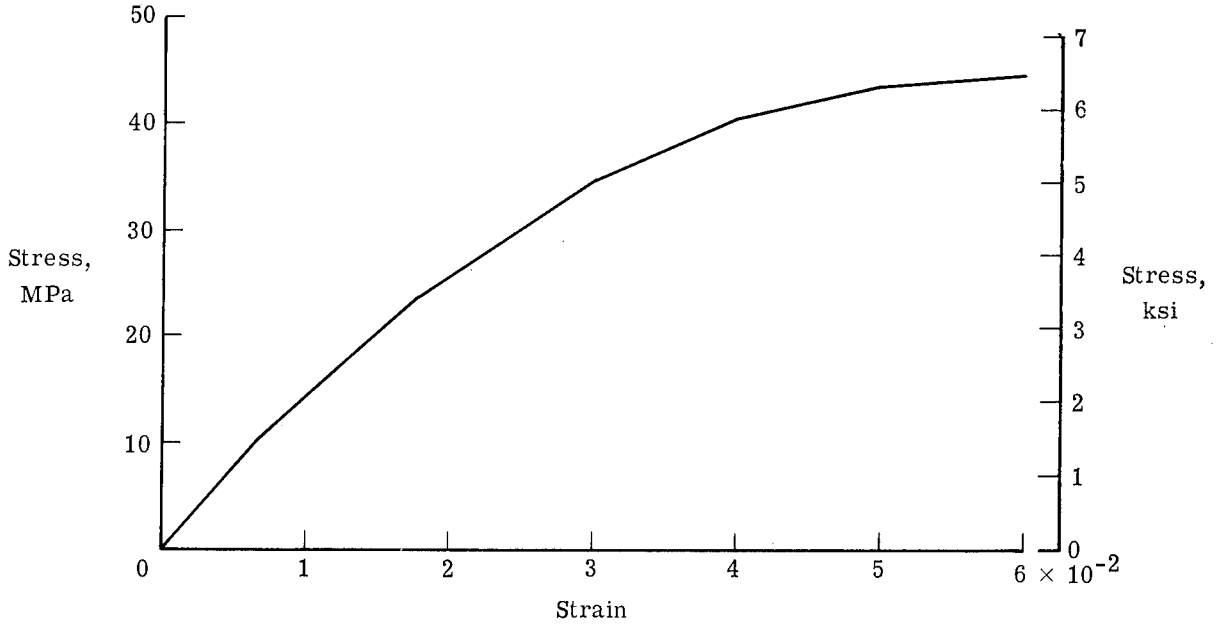

Figure 16.- Assumed stress-strain relationship for inelastic AF-126 adhesive.

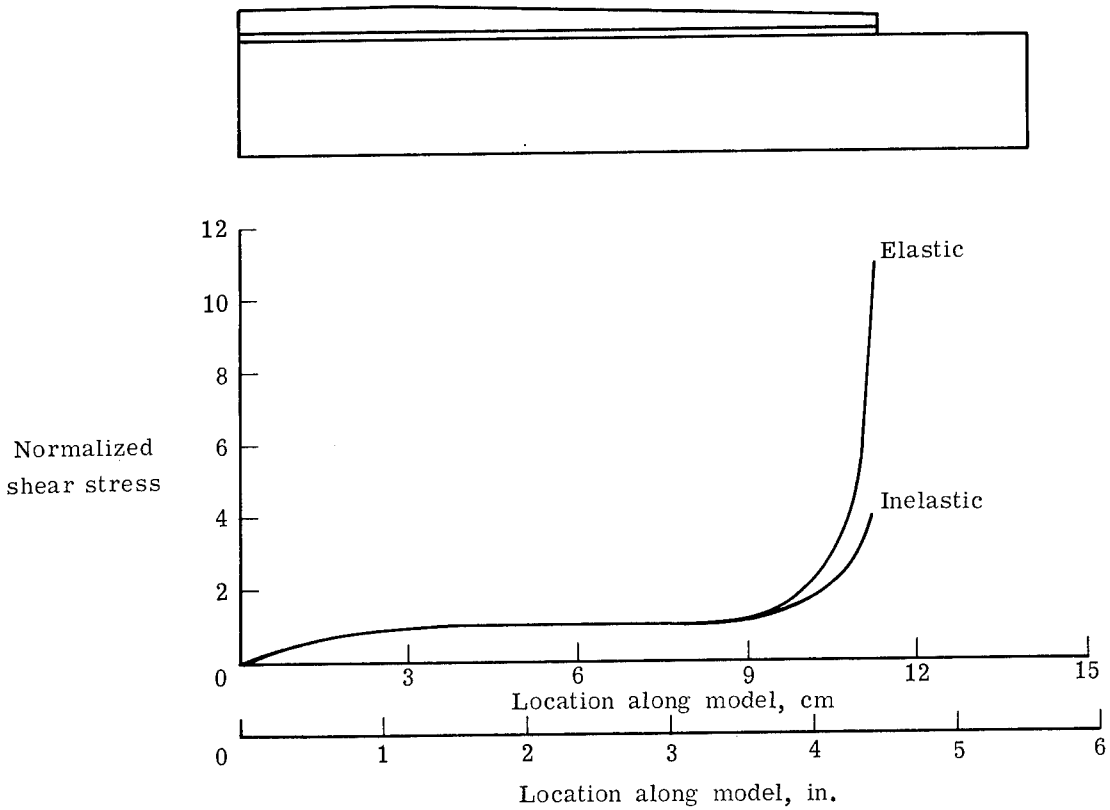

Figure 17.- Comparison of shear stresses in elastic and inelastic adhesive.

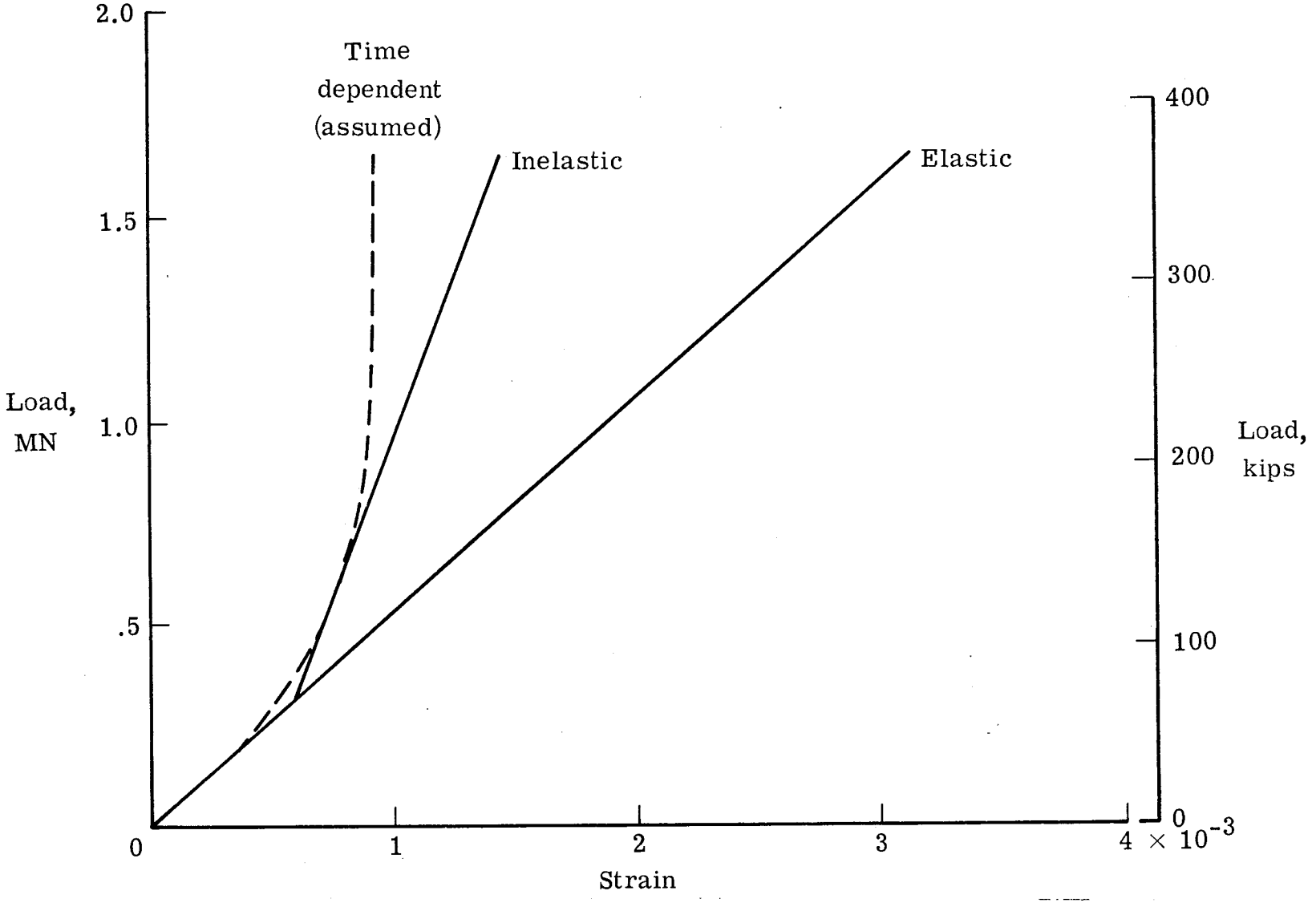

Figure 18.- Decrease in strain in titanium end fitting due to inelastic behavior of adhesive.